Supporting Information

A Universal Double-Side Passivation for High Open-Circuit Voltage in Perovskite Solar Cells: Role of Carbonyl Groups in Poly(methyl methacrylate)

Jun Peng, Jafar I. Khan, Wenzhu Liu, Esma Ugur, The Duong, Yiliang Wu, Heping Shen, Kai Wang, Hoang Dang, Erkan Aydin, Xinbo Yang, Yimao Wan, Klaus J. Weber, Kylie R. Catchpole, Frédéric Laquai, Stefaan De Wolf, Thomas P. White**

Jun Peng, Dr. The Duong, Yiliang Wu, Dr. Heping Shen, Dr. Yimao Wan, A/Prof. Klaus J. Weber, Prof. Kylie R. Catchpole and A/Prof. Thomas P. White
Research School of Engineering, The Australian National University, Canberra, ACT 2601, Australia
E-mail: thomas.white@anu.edu.au

Dr. Jafar I. Khan, Dr. Wenzhu Liu, Esam Ugur, Dr. Kai Wang, Dr. Hoang Dang, Dr. Erkan Aydin, Dr. Xinbo Yang, A/Prof. Frédéric Laquai and A/Prof. Stefaan De Wolf
King Abdullah University of Science and Technology (KAUST), KAUST Solar Center (KSC), Physical Sciences and Engineering Division (PSE), Thuwal 23955-6900, Kingdom of Saudi Arabia
E-mail: stefaan.dewolf@kaust.edu.sa

This Supporting Information includes:

Experimental Section

Perovskite device preparation

(1) FTO/c-In-TiO_x/m-TiO_2 ETLs preparation

FTO substrates (7Ω/□, Dyesol) were sequentially cleaned by detergent, acetone, isopropanol and ethanol in an ultrasonic bath for 10 min each, followed by UV-O_3 treatment for a further 10 min. Next, ~70 nm layers of compact In-TiO_2 were deposited on the pre-cleaned FTO substrates according to the Ref[1]. Mesoporous TiO_2 layers (~90 nm thick) were deposited on the FTO/c-In-TiO_2 compact layer via spin casting meso-TiO_2 paste solution for 30 s at 5000 rpm with a ramp of 5000 rpm s^{-1}. The meso-TiO_2 paste solution was prepared from 30 nm TiO_2 particle paste (30 NR-D, Dyesol) diluted in anhydrous Ethanol (1:9, w/w).

(2) PMMA:PCBM passivation layer deposition

The PMMA:PCBM passivation layer was spin coated on the FTO/c-In-TiO_x/m-TiO_2 according to Ref[2], where the PMMA:PCBM blend solution was prepared by dissolving 1 mg PMMA (Mw~120000, Sigma Aldrich) and 3 mg $PC_{61}BM$ (Sigma Aldrich) into 1 mL Chlorobenzene.

(3) Multi-cation perovskite fabrication and PMMA passivation treatment

The multi-cation $Cs_{0.07}Rb_{0.03}FA_{0.765}MA_{0.135}PbI_{2.55}Br_{0.45}$ perovskite precursor was prepared from 1.2 M lead iodide (PbI_2, 99%, Sigma Aldrich), 1.1 M formamidinium (FAI, Dyesol), 0.2 M lead bromide ($PbBr_2$, 99.999%, Sigma Aldrich), 0.2 M methylamine bromide (MABr, Dyesol), 0.091 M cesium iodide (CsI, 99.999%, Sigma Aldrich), 0.039 M rubidium iodide (RbI, 99.9%, Sigma Aldrich) in 1 mL anhydrous DMF:DMSO (4:1, v/v, Sigma Aldrich) blend solvents.

A two-step spin coating program was used to deposit the perovskite thin films: first at 2000 rpm with a ramp of 200 rpm s^{-1} for 10 s, and then at 5000 rpm with a ramp of 1000 rpm s^{-1} for 25 s. During the second step, approximately 200 µl Chlorobenzene was poured on the

spinning substrate 8 s prior to the end of the program. This was followed by thermal annealing and PMMA passivation treatment for different perovskite samples as follows:

(i) Perovskite control cell (with a structure of FTO/c-In-TiO_x/m-TiO_2/Perovskite/Spiro-OMeTAD/Au). After the two-step spin coating program, the perovskite sample was immediately annealed on a hotplate at 100 ^oC for 30 min.

(ii) Passivated ETL side perovskite cell (with a structure of FTO/c-In-TiO_2/m-TiO_2/PMMA:PCBM/Perovskite/Spiro-OMeTAD/Au). After the two-step spin coating program, the perovskite sample was immediately annealed on a hotplate at 100 ^oC for 30 min.

(iii) Double-side passivated perovskite cell (with a structure of FTO/c-In-TiO_x/m-TiO_2/PMMA:PCBM/Perovskite/PMMA/Spiro-OMeTAD/Au). After the two-step spin coating program, the perovskite sample was immediately annealed on a hotplate at 100 ^oC for 45 s. The sample was then returned to the spin-coater and immediately cooled down by fast rotation at 5000 rpm with a ramp of 5000 rpm s^{-1} for 15 s. Next, the PMMA passivation treatment was applied: first, 50 uL PMMA solution (1 mg/ml in Chlorobenzene) was dropped on top of the perovskite sample and left for 2 s; second, the sample was spin-coated for 15 s at 5000 rpm with a ramp of 5000 rpm s^{-1}; finally, the sample was immediately annealed on a hotplate at 100 ^oC for 30 min.

(4) Spiro-OMeTAD HTL preparation and Gold contact deposition

The Spiro-OMeTAD precursor solution was prepared by dissolving 72.5 mg Spiro-OMeTAD, 28.5 µL 4-tert-butylpyridine and 17.5 µL of lithium bis(trifluoromethanesulfonyl)imide solution (520mg/mL in acetonitrile) in 1 mL Chlorobenzene. Note that after spin-coating (3000 rpm with a ramp of 3000 rpm/s for 30 s) the Spiro-OMeTAD layer, the substrates were placed in air in a humidity-control box for 12 hours to ensure sufficient oxidation of the Spiro-OMeTAD film prior to ~100 nm gold contact layer deposition (thermal evaporation). The effective area of perovskite cells reported in this work is 4 mm x 4 mm (0.16 cm^2)

(well-defined by the rear gold contact that was deposited through a shadow mask). Our perovskite cells were fabricated on substrates of dimension 12.5 mm*14.0 mm. Note that we only had one cell on each substrate.

Perovskite device measurements

J-V measurements. All devices were tested under 1 sun conditions (100 mW/cm^2, AM 1.5G, 25 ^{o}C) in a solar simulator system (model #SS150 from Photo Emission Tech Inc) equipped with a Xenon lamp. The light intensity was calibrated using a certified Fraunhofer CalLab reference cell. For the perovskite solar cells, all *J-V* curves were tested at a 50 mV/s scan rate and at room temperature in a custom-built vacuum measurement jig (without an aperture mask) under air. Note that reverse scan is from V_{oc} to J_{sc} (forward bias → short circuit, 1.25 V → -0.1 V), and forward scan is from J_{sc} to V_{oc} (short circuit → forward bias, -0.1 V → 1.25 V). No preconditioning protocol has been applied before the characterization.

External quantum efficiency (EQE) measurements. External quantum efficiency (EQE) were performed on a commercial EQE system (Newport). For our double-side passivated perovskite cell, the estimated spectrum mismatch correction is 98.45 % based on the comparison between the integrated current density calculated from the EQE response and the current density measured under the solar simulator. No preconditioning protocol has been applied before the characterization.

Characterization

Photoluminescence imaging. For photoluminescence (PL) imaging, the cells were held in a nitrogen-filled and temperature-controlled jig. The jig is mounted in a home-built PL imaging system and uniformly illuminated with two 430 nm royal-blue LED chips, filtered by bandpass filters (451/106 nm). Following illumination (Intensity~100 mW/cm^2), a Peltier-cooled (-70 °C) Si CCD camera (Princeton Instruments Pixis 1024) with a long-pass filter

(750 nm) was used to image the luminescence from the perovskite cells with an exposure time of 0.08 seconds. PL images were taken when cells were under both open circuit and reverse bias (-2 V) conditions. The open circuit images were then subtracted from the reverse bias image to ensure the luminescence emission was solely from the perovskite absorber layer.

X-ray Diffraction (XRD) measurements. X-ray diffraction analysis was performed with a Bruker D8 Advance diffraction meter operated at 30 kV, 10 mA at 2θ (Cu Kα) 10–60°, step 0.02° and scan speed 2.3° min^{-1}.

Scanning Electron Microscope (SEM) measurements. A Nova Nano630 scanning electron microscope (SEM) was used to investigate the surface morphology of samples. A Helios Nanolab 600 FIB system was used to prepare cross-sectional SEM images of the cells.

Transient Absorption (TA) Spectroscopy measurements. Ultrafast pump-probe transient absorption (TA) spectroscopy was performed to reveal the charge carrier dynamics of various samples. All measurements were conducted in the time range from 1 nanosecond (ns) to 100 microseconds (μs). The fundamental output of a titanium:sapphire amplifier, Coherent Legend Duo, operating at 800 nm with a repetition rate of 3 kHz and energy of 4.5 mJ is split into 3 segments (2 mJ, 1 mJ and 1.5 mJ), two of them are used to pump two optical parametric amplifiers (Light conversion TOPAS Prime). One of the TOPAS generates tunable pump pulses, while the second one generates a signal (1300 nm) and idler (2000 nm) only. A fraction of the signal beam of the second TOPAS was focused into a c-cut 3 mm thick CaF2 window, thereby generating a white-light supercontinuum from 350 to 1000 nm. For long delay TA measurement, the probe white-light supercontinuum was used, the excitation (pump pulse) was provided by an actively Q-switched Nd:YVO4 laser (InnoLas picolo AOT) frequency-doubled to provide pulses at 532 nm, and triggered by an electronic delay generator

(Stanford Research Systems DG535), itself triggered by the TTL sync from the Legend DUO, allowing control of the delay between pump and probe with a jitter of roughly 100 ps.

Pump and probe beams were focused to overlap spatially on the sample. The transmitted fraction of the white light was guided to a custom-made prism spectrograph (Entwicklungsbüro Stresing) where it was dispersed by a prism onto a 512 pixel NMOS linear image sensor (Hamamatsu S8381-512). The probe pulse repetition rate was 3 kHz but the excitation was directly generated at 1.5 kHz frequency covering a temporal range from 1 ns to 100 μs delays, while the detector array was read out at 3 kHz. Adjacent diode readings corresponding to the transmission (T) of the sample after excitation and in the absence of an excitation pulse were used to calculate $\Delta T/T$. Measurements were averaged over several thousand shots to obtain a good signal-to-noise ratio. Finally, the chirp induced by the transmissive optics was corrected with a home-built Matlab code by revaluating for each wavelength the delay at which pump and probe are simultaneously arriving on the sample as the time of the signal amplitude. All measurements were performed at room temperature in vacuum.

Time-Resolved Photoluminescence (TR-PL) spectroscopy measurements. For TR-PL experiments samples were excited with the wavelength-tunable output of an OPO (Radiantis Inspire HF-100), itself pumped by the fundamental of a Ti:Sa fs-oscillator (Spectra Physics MaiTai eHP) at 820 nm. The repetition rate of the fs pulses was adjusted by a pulse picker (APE Pulse Select) and typical pulse energies were in the range of several nJ. Photoluminescence was collected by an optical telescope (consisting of two plano-convex lenses), focused on the slit of a spectrograph (PI Spectra Pro SP2300) and detected with a Streak Camera (Hamamatsu C10910) system with a temporal resolution of 1.4 ps.

Fourier-Transform Infrared (FTIR) Spectroscopy measurements. FTIR spectroscopy of pure PMMA, PMMA + PbI_2, PMMA + PbI_2 + $PbBr_2$ and PMMA + FAI thin film samples were performed using a commercial FTIR system (Cary 680, Agilent) in transmission mode. All samples were fabricated by spin-coating their corresponding precursor solutions at 500 rpm for 60 s, then placed in a vacuum chamber to remove the residual solvents. The precursor solution for the pure PMMA sample was prepared by dissolving 50 mg PMMA powder into 1 mL DMSO. The precursor solution for PMMA + PbI_2 sample was prepared by dissolving 25 mg PMMA and 40 mg PbI_2 into 1 mL DMSO. The precursor solution of PMMA + PbI_2 + $PbBr_2$ sample was prepared by dissolving 25 mg PMMA + 34 mg PbI_2 + 6 mg $PbBr_2$ into 1 mL DMSO. The precursor solution for the PMMA + FAI sample was prepared by dissolving 25 mg PMMA and 40 mg FAI into 1 mL DMSO.

Nuclear Magnetic Resonance (NMR) Spectroscopy measurements. NMR spectroscopy carried out with a Bruker Avance III Ultrashield Plus instrument using a 400 MHz proton frequency at room temperature. The spectra were measured at DMSO-d6 with TMS as an internal standard. The PMMA sample was measured at 10 mg/ml; the PMMA + PbI_2 sample was measured at 5 mg/ml for PMMA and 20 mg/ml for PbI_2; the PMMA + FAI sample was measured at 5 mg/ml for PMMA and 20 mg/ml for FAI.

First-Principles Calculations. First-principles calculations: The DFT calculations were performed using the Dmol3 module[3,4] in Materials Studio 2017 R2 package (Accelrys, SanDiego, CA). The DNP 4.4 basis set was employed to describe electronic charge density and electrostatic potential. The basis set cutoff is 3.3 Å during the geometrical optimization,[5,6] where the convergence tolerance is 2×10^{-5} Ha for the energy, 0.004 Ha $Å^{-1}$ for the forces, and 0.005 Å for the displacement. The electronic self-consistence field (SCF)

tolerance is set to 10^{-5} Ha. The exchange correlation adopted the general gradient approximation, Perdew–Burke–Ernzerhof (GGA-PBE) functional.[7]

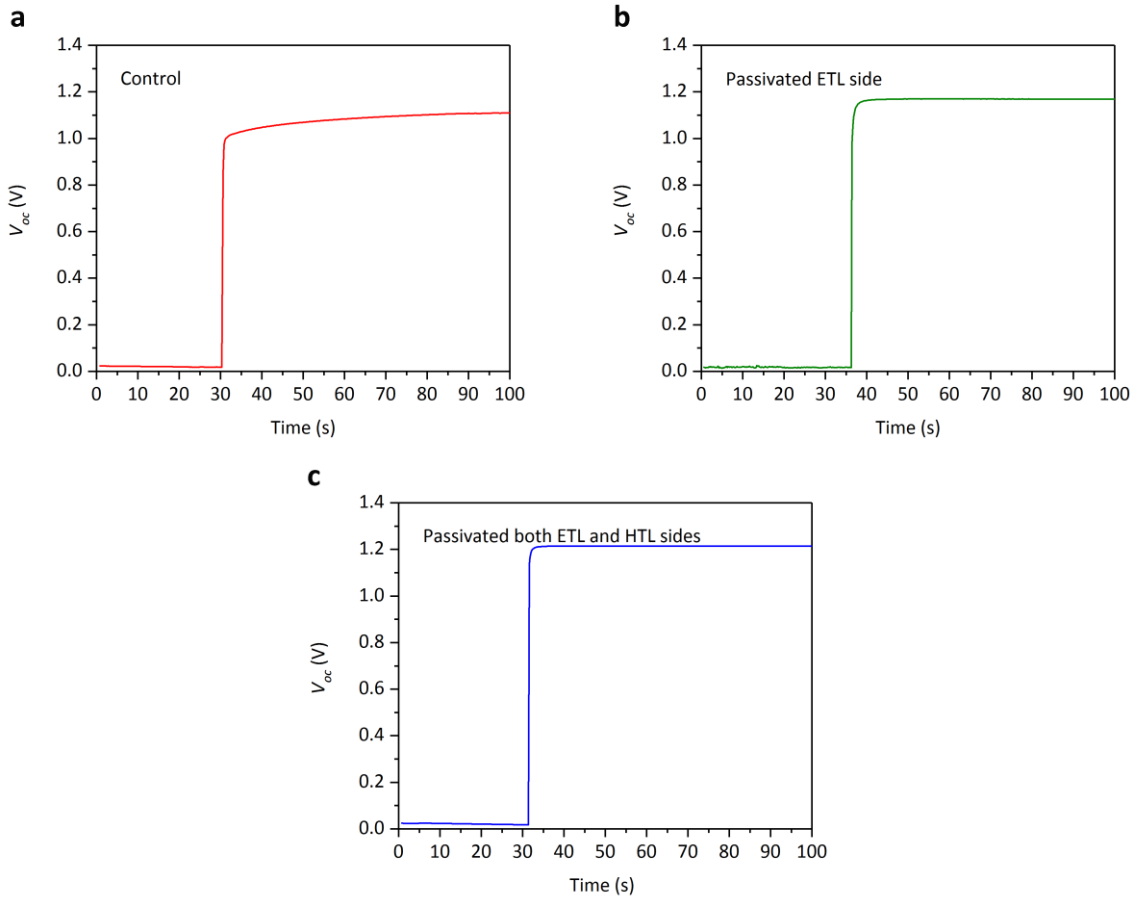

Figure S1. The V_{oc} response of the control and passivated perovskite cells with/without PMMA:PCBM and PMMA passivation layer tested under open circuit condition. a). Control cell, with a structure of FTO/c-In-TiO_x/m-TiO_2/Perovskite/Spiro-OMeTAD/Au. b) Passivated ETL side cell, with a structure of FTO/c-In-TiO_x/m-TiO_2/PMMA:PCBM/Perovskite/Spiro-OMeTAD/Au. c) Double-side passivated cell, with a structure of FTO/c-In-TiO_x/m-TiO_2/PMMA:PCBM/Perovskite/PMMA/Spiro-OMeTAD/Au. Note that 'perovskite' represents $Cs_{0.07}Rb_{0.03}FA_{0.765}MA_{0.135}PbI_{2.55}Br_{0.45}$.

As seen in Figure S1, the V_{oc} of the control cell took around 50 s to reach a steady-state maximum V_{oc} condition, while for the passivated ETL side perovskite cell and the double-side passivated cell the response time was significantly reduced to 2-3 s.

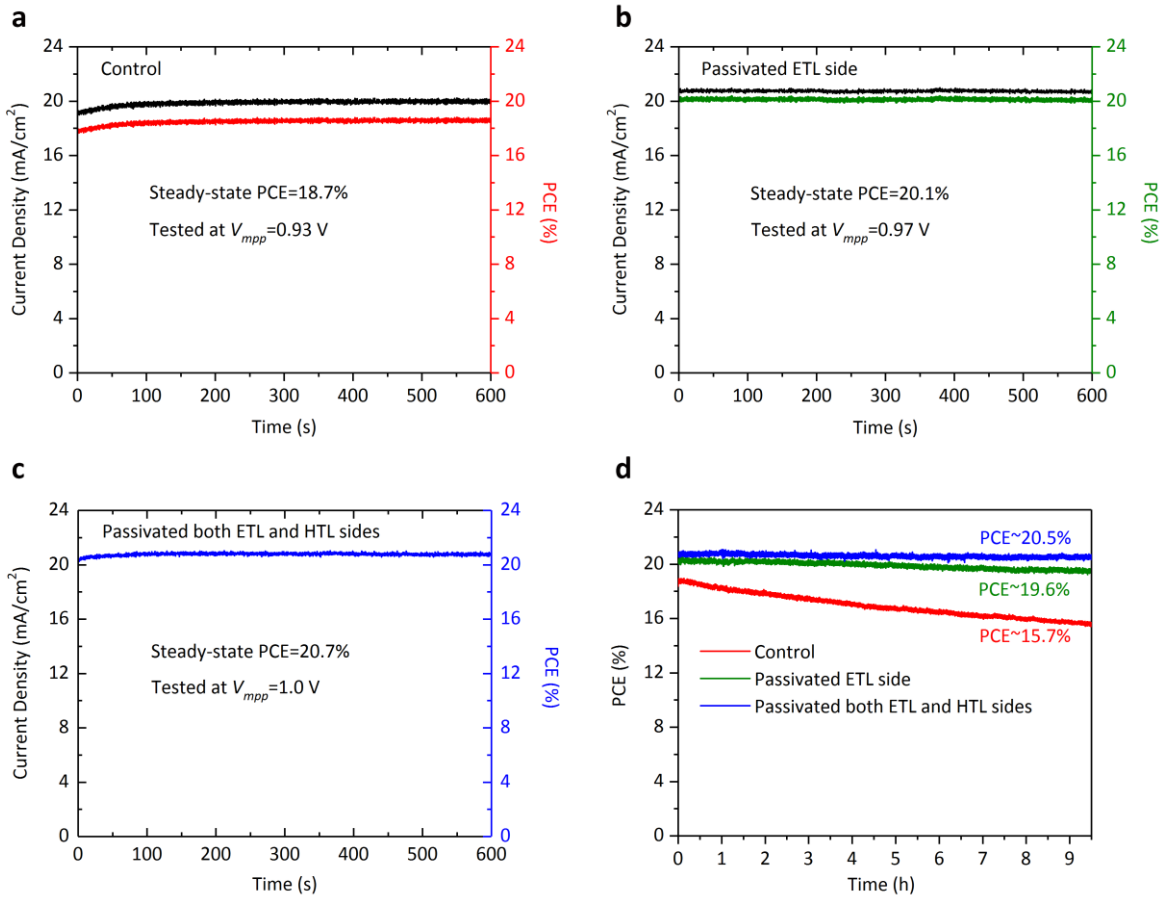

Figure S2. The steady-state PCE of the control and passivated perovskite cells with/without PMMA:PCBM and PMMA passivation layer tested at V_{mpp}. a). Control cell, with a structure of FTO/c-In-TiO_x/m-TiO_2/Perovskite/Spiro-OMeTAD/Au. b) Passivated ETL side cell, with a structure of FTO/c-In-TiO_x/m-TiO_2/PMMA:PCBM/Perovskite/Spiro-OMeTAD/Au. c) Double-side passivated cell, with a structure of FTO/c-In-TiO_x/m-TiO_2/PMMA:PCBM/Perovskite/PMMA/Spiro-OMeTAD/Au. d) Steady-state PCE tests measured over a period of 9.5 hours. Note that 'perovskite' represents $Cs_{0.07}Rb_{0.03}FA_{0.765}MA_{0.135}PbI_{2.55}Br_{0.45}$.

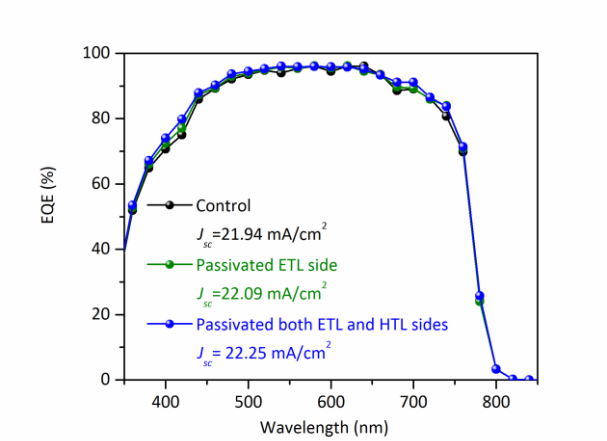

Figure S3. EQE measurements for the control, passivated ETL side and double-side passivated cells. The control cell structure is FTO/c-In-TiO_x/m-TiO_2/Perovskite/Spiro-OMeTAD/Au; passivated ETL side cell structure is FTO/c-In-TiO_x/m-TiO_2/PMMA:PCBM/Perovskite/Spiro-OMeTAD/Au; double-side passivated cell structure is FTO/c-In-TiO_x/m-TiO_2/PMMA:PCBM/Perovskite/PMMA/Spiro-OMeTAD/Au. Note that 'perovskite' represents $Cs_{0.07}Rb_{0.03}FA_{0.765}MA_{0.135}PbI_{2.55}Br_{0.45}$.

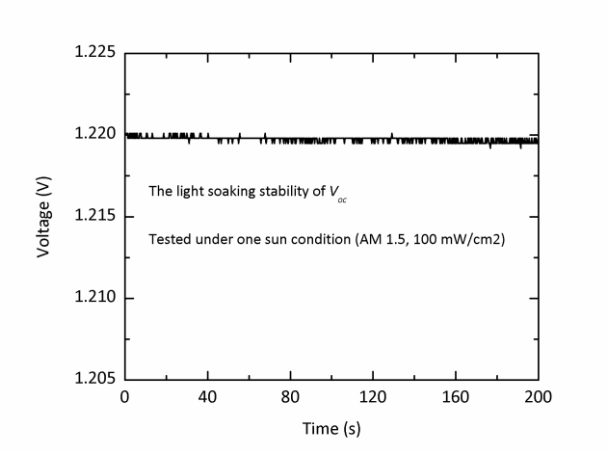

Figure S4. The light soaking stability of the open-circuit voltage (V_{oc}) of our double-side passivated perovskite cell tested under one sun condition (AM 1.5, 100 mW/cm^2).

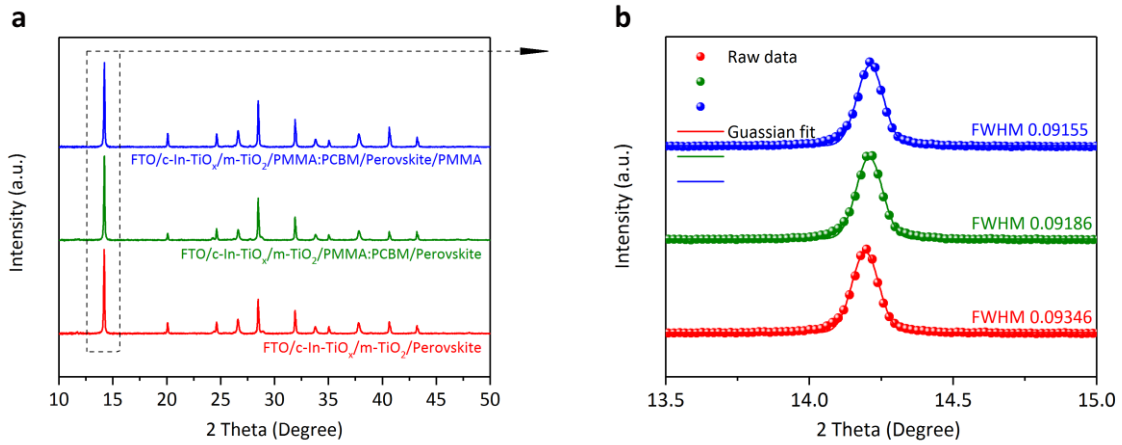

Figure S5. a) XRD spectra of the perovskite thin films deposited on different FTO/c-In-TiO_x/m-TiO_2 substrates with/without the PMMA:PCBM and PMMA passivation layer. b) The corresponding Gaussian fit of the dominant black perovskite phase for perovskite thin film. Note that the perovskite composition is $Cs_{0.07}Rb_{0.03}FA_{0.765}MA_{0.135}PbI_{2.55}Br_{0.45}$.

In Figure S5a, the XRD spectra show no systematic variations for perovskite samples with/without PMMA:PCBM or PMMA passivation layers, and no obvious PbI_2 or other non-perovskite phases. To further investigate the crystallite size of perovskite, the dominant black perovskite phase is fitted with a Gaussian distribution to determine the full width at half maximum (FWHM) for each sample. As presented in the Figure S5b, it reveals that the value of FWHM for FTO/c-In-TiO_x/m-TiO_2/perovskite sample is 0.09346, while the values of FWHM for FTO/c-In-TiO_x/m-TiO_2/PMMA:PCBM/Perovskite and FTO/c-In-TiO_x/m-TiO_2/PMMA:PCBM/Perovskite/PMMA samples are 0.09186 and 0.09155 respectively. As expected, there are no significant variations for the crystallite size of perovskite deposited on different substrates with/without PMMA:PCBM and PMMA passivation layer based on the calculated FWHM.

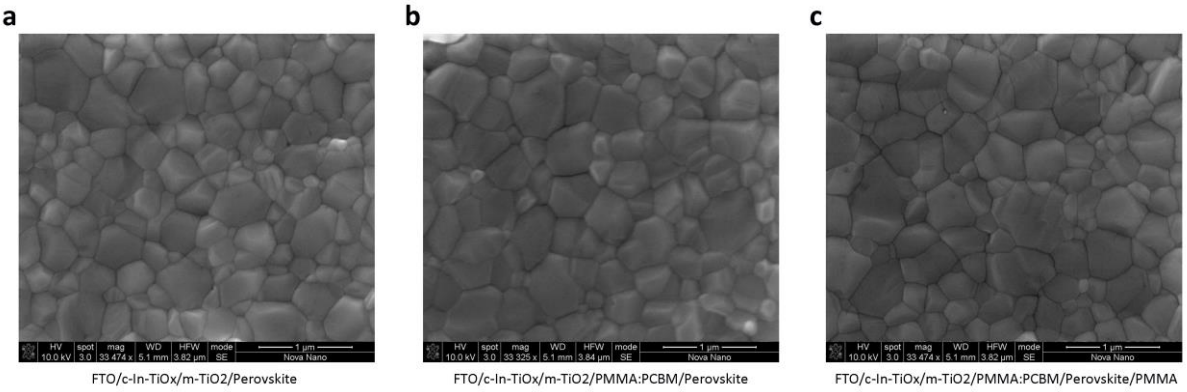

Figure S6. SEM images for different samples: a) FTO/c-In-TiO_x/m-TiO_2/Perovskite; b) FTO/c-In-TiO_x/m-TiO_2/PMMA:PCBM/Perovskite; c) FTO/c-In-TiO_x/m-TiO_2/PMMA:PCBM/Perovskite/PMMA. Note that the perovskite represents $Cs_{0.07}Rb_{0.03}FA_{0.765}MA_{0.135}PbI_{2.55}Br_{0.45}$.

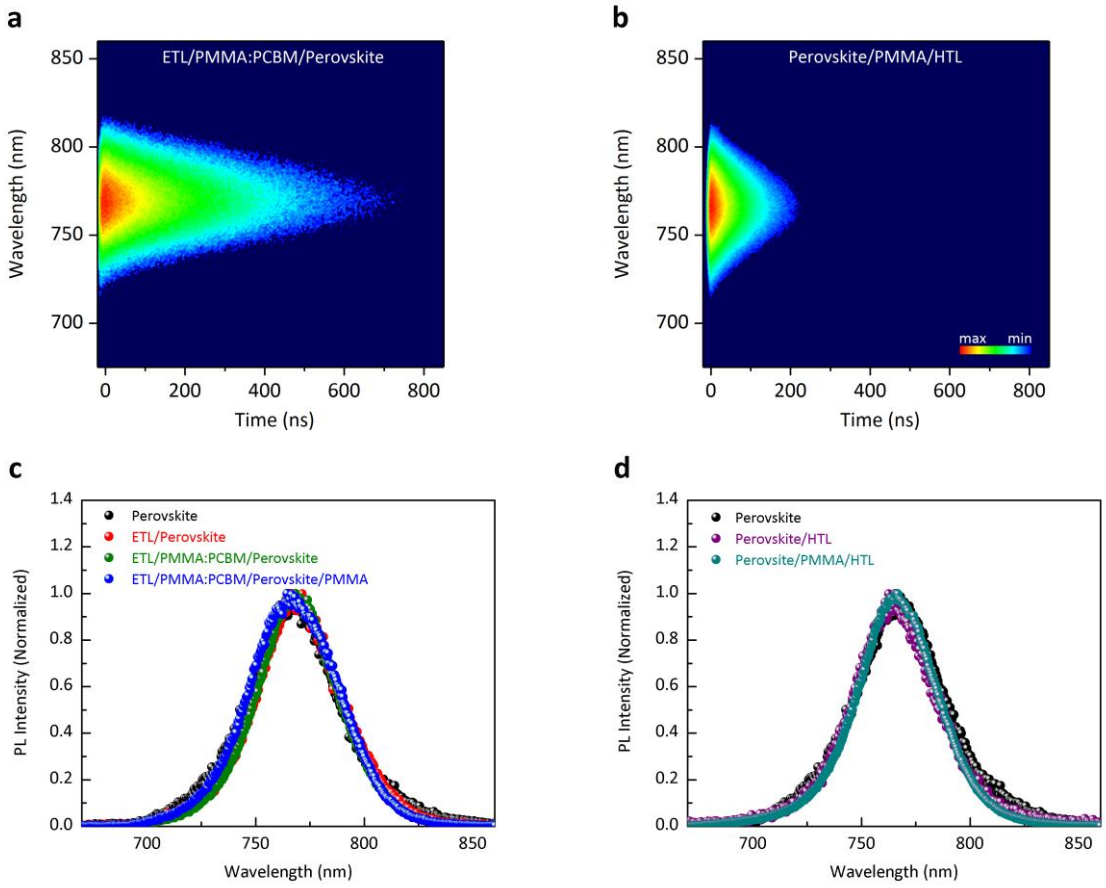

Figure S7. a) TR-PL data for ETL/PMMA:PCBM/Perovskite after excitation at 650 nm. b) TR-PL data for Perovksite/PMMA/HTL samples after excitation at 650 nm. c) The acquired TR-PL spectra of Perovskite, ETL/Perovskite, ETL/PMMA:PCBM/Perovskite and ETL/PMMA:PCBM/Perovskite/PMMA samples with the characteristic peak at 770 nm. d) TR-PL spectra of Perovskite, Perovskite/HTL and Perovskite/PMMA/HTL samples with the characteristic peak at 770 nm. Note that all samples were fabricated on high-grade optical quartz substrates. And the ETL, HTL and Perovskite represent c-In-TiO_x/m-TiO_2, Spiro-OMeTAD and $Cs_{0.07}Rb_{0.03}FA_{0.765}MA_{0.135}PbI_{2.55}Br_{0.45}$, respectively.

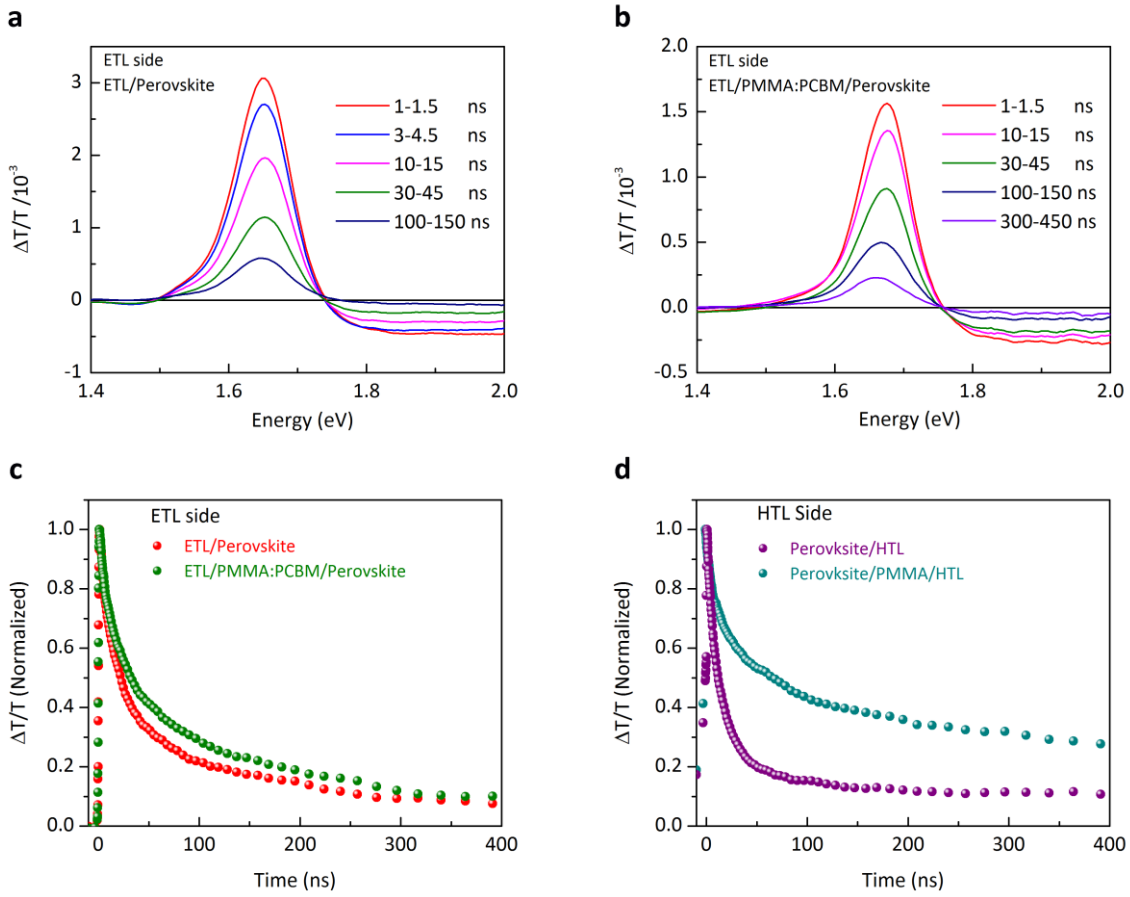

Figure S8. Transient absorption (TA) spectra of: a) ETL only samples (illuminated from the ETL side): ETL/perovskite; b) ETL only samples (illuminated from the ETL side): ETL/PMMA:PCBM/Perovskite. ns-µs dynamics of TA data monitored at the position of the ground state bleach: c) ETL only samples (illuminated from the ETL side): ETL/perovskite and ETL/PMMA:PCBM/Perovskite; d) HTL only samples (illuminated from the HTL side): perovsite/HTL and perovskite/PMMA/HTL. Note that all samples were fabricated on high-grade optical quartz substrates. ETL, HTL and perovskite represent c-In-TiO_x/m-TiO_2, Spiro-OMeTAD and $Cs_{0.07}Rb_{0.03}FA_{0.765}MA_{0.135}PbI_{2.55}Br_{0.45}$, respectively.

The recombination dynamics were also determined by transient absorption (TA) spectroscopy in the nano-to-microsecond time range, using a 532 nm laser as excitation source (corresponding to an absorption depth into the perovskite layer of around 100 nm). As the thickness of the perovskite absorber layer is 300 nm, this technique thus will mostly monitor the recombination dynamics close to the excited side of the sample. The spectral evolution is depicted in Figure S8, showing the typical narrow peak at 1.65 eV, which is a convolution of

the ground state bleach (GSB) band of the perovskite and stimulated emission, whereas a broad photo-induced absorption (PIA) band spans the spectral range of 1.75 eV-2.25 eV. The data shows that when illuminating from the ETL-side the signal decays slower for the passivated sample (more than 450 ns), compared to the control sample (about 200 ns). Figure S8c shows the normalized kinetics of the GSB recovery for these samples, underlining again the beneficial effect of passivation. Interestingly, when illuminating from the HTL side (see Figure S8d), the passivated sample clearly exhibits a much slower dynamics with 40 % of the signal still remaining after 200 ns, while only 10 % is left for the case of the reference sample (without passivation). We attribute this to reduced recombination at the HTL/perovskite interface due to the passivation effect of the PMMA layer.

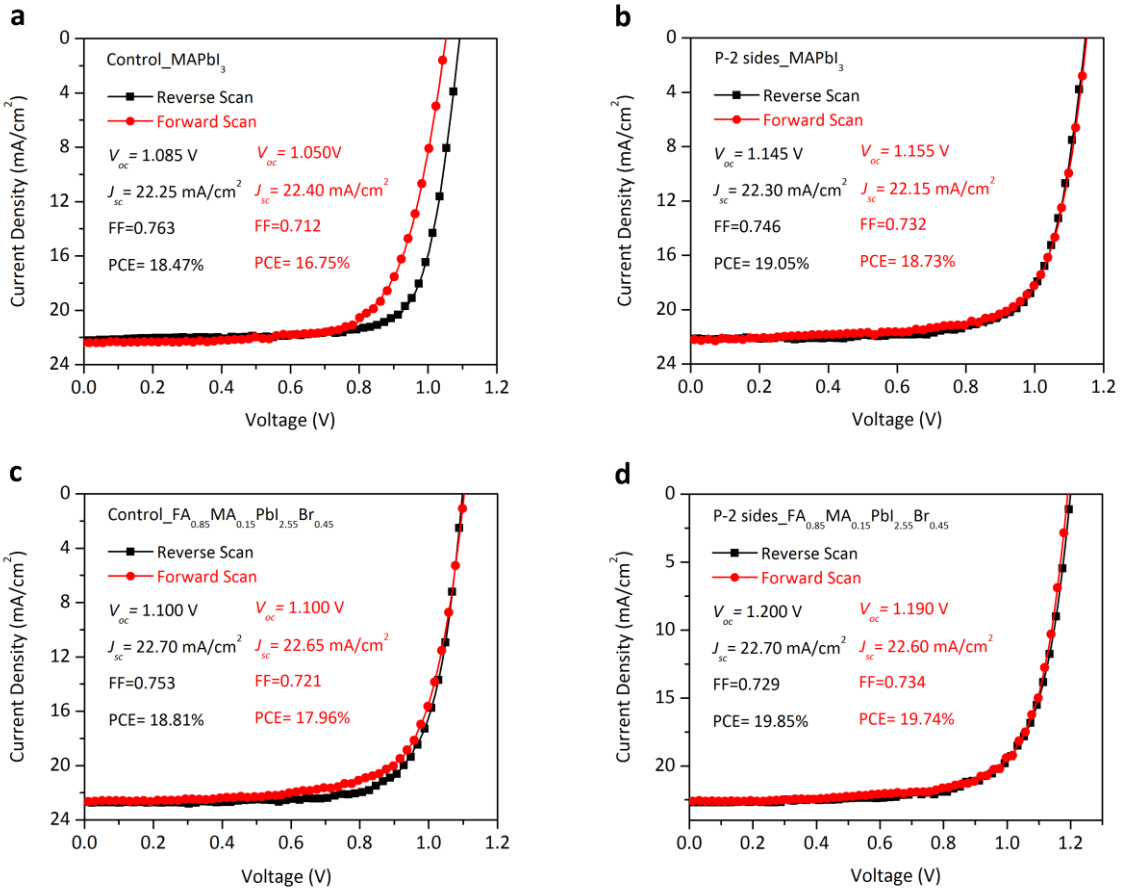

Figure S9. Forward- and reverse-scan *J-V* curves of different perovskite cells. a) Control_$MAPbI_3$ with a structure of FTO/c-In-TiO_x/m-TiO_2/$MAPbI_3$/Spiro-OMeTAD/Au. b) P-2 sides_$MAPbI_3$ with a structure of FTO/c-In-TiO_x/m-TiO_2/PMMA:PCBM/$MAPbI_3$/PMMA/Spiro-OMeTAD/Au. c) Control_$FA_{0.85}MA_{0.15}PbI_{0.25}Br_{0.45}$ with a structure of FTO/c-In-TiO_x/m-TiO_2/$FA_{0.85}MA_{0.15}PbI_{0.25}Br_{0.45}$/Spiro-OMeTAD/Au. d) P-2 sides_ $FA_{0.85}MA_{0.15}PbI_{0.25}Br_{0.45}$ with a structure of FTO/c-In-TiO_x/m-TiO_2/PMMA:PCBM/ $FA_{0.85}MA_{0.15}PbI_{0.25}Br_{0.45}$/PMMA/Spiro-OMeTAD/Au. Note that all devices were tested at a scan rate of 50 mV/s.

Table S1. Summary of the detailed photovoltaic parameters of different perovskite cells.

Perovskite	Device Type	Scan Direction	V_{oc} (V)	J_{sc} (mA/cm^2)	FF	PCE (%)
$MAPbI_3$	Control	RS	1.085	22.25	0.763	18.47
		FS	1.050	22.40	0.712	16.75
	P-2 sides	RS	1.145	22.30	0.746	19.05
		FS	1.155	22.15	0.732	18.73
$FA_{0.85}MA_{0.15}PbI_{2.55}Br_{0.45}$	Control	RS	1.100	22.70	0.753	18.81
		FS	1.100	22.65	0.721	17.96
	P-2 sides	RS	1.200	22.70	0.729	19.85
		FS	1.190	22.60	0.734	19.74
$Cs_{0.07}Rb_{0.03}FA_{0.765}MA_{0.135}PbI_{2.55}Br_{0.45}$	Control	RS	1.110	22.85	0.770	19.50
		FS	1.100	22.81	0.738	18.50
	P-2 sides	RS	1.205	22.60	0.764	20.80
		FS	1.213	22.60	0.761	20.86

References

[1] J. Peng, T. Duong, X. Zhou, H. Shen, Y. Wu, H. K. Mulmudi, Y. Wan, D. Zhong, J. Li and T. Tsuzuki, K. J. Weber, K. R. Catchpole and T. P. White, *Adv. Energy Mater*. **2017**, *7*, 1601768.

[2] J. Peng, Y. Wu, W. Ye, D. A. Jacobs, H. Shen, X. Fu, Y. Wan, N. Wu, C. Barugkin and H. T. Nguyen, D. Zhong, J. Li, T. Lu, Y. Liu, M. N. Lockrey, K. J. Weber, K. R. Catchpole and T. P. White, *Energy Environ. Sci.* **2017**, *10*, 1792.

[3] B. Delley, *J. Chem. Phys.* **1990**, *92*, 508.

[4] B. Delley, *J. Chem. Phys.* **2000**, *113*, 7756.

[5] J. Baker, A. Kessi and B. Delley, *J. Chem. Phys.* **1996**, *105*, 192.

[6] J. Andzelm, R. King-Smith and G. Fitzgerald, *Chem. Phys. Lett.* **2001**, *335*, 321.

[7] J. P. Perdew, K. Burke and M. Ernzerhof, *Phys. Rev. Lett.* **1996**, *77*, 3865.